2026 IEEE/SICE International Symposium on System Integration (SII)
January 11-14, 2026. Cancún, México

Impact Attenuation in Robotic Hammering Tasks

Haruto Ueda[1] and Ryo Kikuuwe[1]

***Abstract*— This paper proposes a control method for robotic hammering that can attenuate the reaction torques on the robot's joints while maintaining a sufficient impact on the environment. A key challenge in hammering tasks is this trade-off between delivering a sufficient impact and preventing damage to the manipulator. The proposed method addresses this conflict by generating the entire pre-collision trajectory, including the required initial posture, by calculating backward in time from a desired state at the moment of impact. The trajectory consists of a preparatory backswing and a striking motion, both tracked using a PD controller. To further attenuate reaction torques, a feedforward torque pulse is applied to the final joint just before impact. After impact, a force-controlled lift-up mode is activated to raise the hammer and return the robot to its initial posture. The effectiveness of the proposed method is validated through experiments, demonstrating an attenuation in joint torque.**

I. Introduction

Robot arms are installed on factory production lines for automation purposes and are utilized in various industries, including the automotive, semiconductor, electronic device, and food industries. The majority of robot arm applications involve tasks such as welding and material handling; their implementation for tasks involving impulsive forces has not occurred.

Generally, most industrial robot arms are controlled by a dedicated position controller, operating based on position commands from high-level controllers. This type of industrial position servo equipment has undisclosed internal control laws and exhibits delays stemming from sensor signals, position command signals, and the elasticity and friction of the gear transmission. Consequently, most industrial position servo systems are unsuitable for tasks that involve impulsive forces. Tasks involving impulsive forces may cause damage to the hardware by persistently applying excessive contact forces to the robot and destabilizing the control system, which leads to excessive vibration. These challenges hinder the adoption of industrial robots for operations involving impulsive forces.

In recent years, some studies have focused on the impact. Dehio et al. [1] proposed a method for grasping and lifting an object at maximum speed using two robotic arms, without violating the constraints derived from hardware limitations and kinematic models. Wang et al. [2] proposed a technique for accurately predicting the impact applied to a robot based on the pre-collision velocity. Van Steen et al. [3] proposed a method for optimizing jumping and landing in quadruped robots by modeling the robot as a spring-loaded inverted pendulum and controlling the robot such that its center of gravity follows a precomputed trajectory. Li et al. [4] proposed a novel admittance controller to address instability when impacting environments with unknown stiffness.

This paper proposes a control method for hammering tasks such as nailing. The key difficulty in these tasks lies in a trade-off: delivering a sufficient impulsive force to the environment and suppressing the reaction torques applied to the robot's joints to prevent damage. The proposed method resolves this conflict by generating a trajectory that can be adapted to any given target position. This trajectory is designed to deliver a sufficient impulsive force to the target while preventing damage to the manipulator.

II. Approach

Realizing hammering tasks with a robotic arm requires applying a sufficient force to the environment while suppressing the forces transmitted to the robot itself.

The interaction between the hammer and the gear transmission of the robot's wrist joint can be modeled as shown in Fig. 1. Here, the gear transmission is represented by two carts, following the model proposed by Kikuuwe [5]. The hammer's displacement is denoted by p and the joint's (rotational) displacement is denoted by q. As the input and output gears are meshed, the corresponding carts slide against each other at their contact surface without separating from each other. It is therefore assumed that the normal force between the carts can be either positive or negative. For example, when a command force pulls the input cart upward, the normal force λ_n from the input shaft to the output shaft acts on the output cart in the upper-right direction, causing it to move to the right. Conversely, when the input cart moves

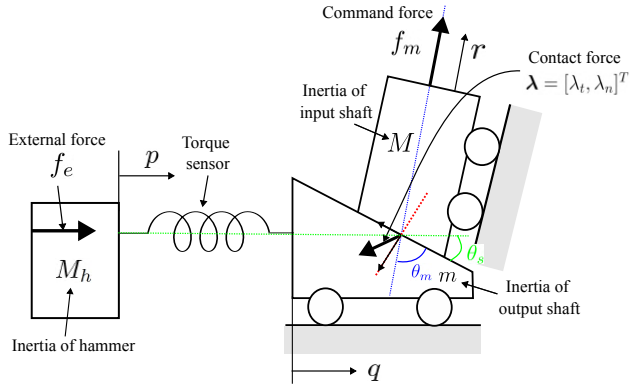

Fig. 1. Physical model of a hammer hitting the wrist joint equipped with a gear transmission.

*This work was supported by JSPS KAKENHI Grant Number 24K00836.

[1]Machinery Dynamics Laboratory, Hiroshima University, 1-4-1 Kagamiyama, Higashi-Hiroshima, Hiroshima 739-8527, Japan. (e-mail:ueda@mdl.hiroshima-u.ac.jp; kikuuwe@ieee.org)

downward, the normal force λ_n from the input shaft to the output shaft acts downward, causing the output cart to move to the left. Furthermore, the torque sensor is modeled as a spring with stiffness k and zero natural length, and the force f_s applied to the spring is considered the measured force.

The equations of motion for the hammer, input cart, and output cart, as well as the measured force f_s, are given as follows:

$$M_h\ddot{p} = f_e - f_s \tag{1}$$
$$m\ddot{q} = f_s - \lambda_t \cos\theta_s - \lambda_n \sin\theta_s \tag{2}$$
$$M\ddot{r} = f_m - \lambda_t \cos\theta_m + \lambda_n \sin\theta_m \tag{3}$$
$$f_s = k(q - p) \tag{4}$$

where M_h, m, and M are the inertia of the hammer, output cart, and input cart, respectively; p, q, and r are their positions; f_e is the external force on the hammer, and f_m is the command force; and θ_s and θ_m are the angles between the contact surface and the directions of the measured and command forces, respectively.

From the above equations, during hammering, the external force on the hammer is transmitted through the torque sensor to the output cart, pushing it to the right. Consequently, the input cart receives a normal force λ_n from the output cart and is pushed upward. At the same time, a friction force λ_t acts on the input cart, pulling it in the lower-right direction. Therefore, applying an upward command force can reduce the friction force λ_t, allowing the output cart to move more easily in response to the external force. As a result, the measured force f_s is expected to be attenuated.

In addition, assuming the rightward direction is positive, the ideal situation is the one where the spring between the hammer and the output cart remains at its natural length, such that $q - p = 0$ and the measured force f_s is zero. If an external force is applied to the hammer and f_s becomes positive, it indicates a large force is being transmitted to the robot, which could cause damage. Conversely, if f_s is negative, an inertial force is applied as the robot pulls away from the hammer.

Therefore, to maintain this ideal state, the robot's end-effector must be controlled to follow the hammer's motion when it is subjected to an external force. For an instantaneous external force, the impulse-momentum relationship for the hammer is given by:

$$M_h\dot{p}_{\text{pre}} = M_h\dot{p}_{\text{post}} + P \tag{5}$$

where P is the external impulse applied to the hammer, and $\dot{p}_{\text{pre}}$ and $\dot{p}_{\text{post}}$ are the hammer's velocities immediately before and after this impulse is applied, respectively.

Based on this principle, if the velocity of the output cart $\dot{q}$ can be controlled to match the hammer's post-impulse velocity $\dot{p}_{\text{post}}$, the measured force f_s should theoretically remain zero. By providing a command torque τ_m that achieves this condition ($\dot{q} = \dot{p}_{\text{post}}$), no force from the external disturbance will be transmitted to the robot itself.

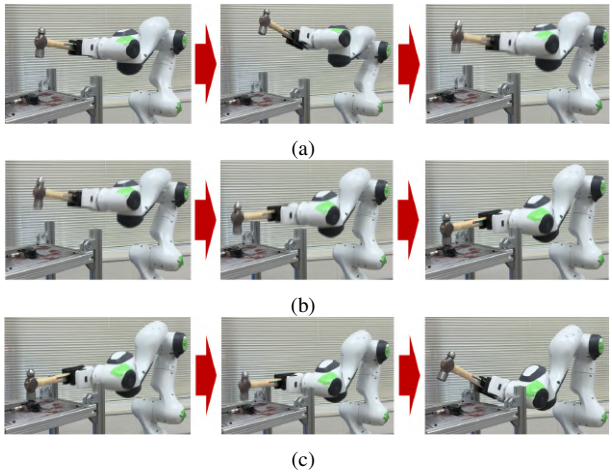

Fig. 2. Mode Transition. (a) Backswing Mode (M1). (b) Striking Mode (M2). (c) Lift-up Mode (M3).

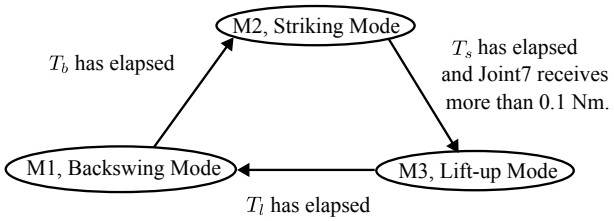

Fig. 3. Mode Transition Diagram.

III. Control Method

A. Hammering Motion

In the proposed method, a complete hammering motion is generated from three key inputs: the planned time T_h of impact, the joint angles $\boldsymbol{q}_t$ at the hit time T_h, and the desired hammer-tip velocity $\boldsymbol{v}_t$. This is achieved by calculating the entire pre-collision trajectory, including the required initial posture $\boldsymbol{q}_{\text{ini}}$, backward in time from these inputs. The resulting motion is divided into three sequential modes, as shown in Fig.2: a backswing mode M1, a striking mode M2, and a post-collision lift-up mode M3. As shown in Fig. 3, the transition from M1 to M2 is time-based, while the switch to M3 is triggered when the measured torque at the 7th joint exceeds 0.1 Nm; ideally, this occurs at the planned time T_h of impact. The trajectories for M1 and M2 are generated using polynomial functions, while M3 utilizes force control instead of trajectory tracking.

B. Mode M2: Striking Mode

The trajectory for M2 is planned first by working backward from the desired state at the planned time T_h of impact. The desired joint angular velocity $\dot{\boldsymbol{q}}_t \in \mathbb{R}^7$ at the hit time, which is calculated from the desired hammer-tip velocity $\boldsymbol{v}_t \in \mathbb{R}^6$. Given the known joint angles $\boldsymbol{q}_t$ at the hit time T_h, this relationship is expressed using the Jacobian $\boldsymbol{J}(\boldsymbol{q}_t)$ as follows:

$$\boldsymbol{v}_t = \boldsymbol{J}(\boldsymbol{q}_t)\dot{\boldsymbol{q}}_t \tag{6}$$

To attenuate the reaction force, a pulse-shaped command torque is applied to the 7th joint in the hammer-lifting direction immediately before impact. However, the experimental hardware has a constraint that the time derivative of the command torque must be within $\pm$ 1000 Nm/s. To apply the torque pulse as intended under this constraint, this paper keeps the 7th joint at its initial angle $q_{\text{ini},7}$ until just before the pulse is applied. Therefore, the desired angular velocity of the 7th joint $\dot{q}_{t,7}$s at the time T_h of impact is set to 0. To reflect this condition, the previously mentioned Eq. (6) is modified.

$$\begin{bmatrix} \dot{x}_t \\ \dot{y}_t \\ \dot{z}_t \\ \omega_{xt} \\ \omega_{zt} \\ \omega_{yt} \end{bmatrix} = \begin{bmatrix} J_{1,1} & J_{1,2} & J_{1,3} & J_{1,4} & J_{1,6} & J_{1,7} \\ J_{2,1} & J_{2,2} & J_{2,3} & J_{2,4} & J_{2,6} & J_{2,7} \\ J_{3,1} & J_{3,2} & J_{3,3} & J_{3,4} & J_{3,6} & J_{3,7} \\ J_{4,1} & J_{4,2} & J_{4,3} & J_{4,4} & J_{4,6} & J_{4,7} \\ J_{6,1} & J_{6,2} & J_{6,3} & J_{6,4} & J_{6,6} & J_{6,7} \\ J_{5,1} & J_{5,2} & J_{5,3} & J_{5,4} & J_{5,6} & J_{5,7} \end{bmatrix} \begin{bmatrix} \dot{q}_{t,1} \\ \dot{q}_{t,2} \\ \dot{q}_{t,3} \\ \dot{q}_{t,4} \\ \dot{q}_{t,6} \\ \dot{q}_{t,7} \end{bmatrix} \tag{7a}$$

Here, $\boldsymbol{v}_{\text{t}}$ is defined as $\boldsymbol{v}_{\text{t}} = [\dot{x}_{\text{t}},\ \dot{y}_{\text{t}},\ \dot{z}_{\text{t}},\ \omega_{\text{xt}},\ \omega_{\text{yt}},\ \omega_{\text{zt}}]^T$, and $\dot{\boldsymbol{q}}_t$ is defined as $\dot{\boldsymbol{q}}_t = [\dot{q}_{t,1}, \dot{q}_{t,2}, \dot{q}_{t,3}, \dot{q}_{t,4}, \dot{q}_{t,6}, \dot{q}_{t,7}]^T$.

First, Eq. (7a) is rearranged by swapping the term ω_{yt} on the left-hand side with the term containing $\dot{q}_{t,7}$ on the right-hand side. Specifically, the equation is transformed from $\omega_{\text{yt}} = J_{5,1}\dot{q}_{t,1} + J_{5,2}\dot{q}_{t,2} + J_{5,3}\dot{q}_{t,3} + J_{5,4}\dot{q}_{t,4} + J_{5,6}\dot{q}_{t,6} + J_{5,7}\dot{q}_{t,7}$ to the form $J_{5,7}\dot{q}_{t,7} = \omega_{\text{yt}} - J_{5,1}\dot{q}_{t,1} - J_{5,2}\dot{q}_{t,2} - J_{5,3}\dot{q}_{t,3} - J_{5,4}\dot{q}_{t,4} - J_{5,6}\dot{q}_{t,6}$.

$$\begin{bmatrix} & -J_{1,7} \\ & -J_{2,7} \\ \boldsymbol{I}_5 & -J_{3,7} \\ & -J_{4,7} \\ & -J_{6,7} \\ \boldsymbol{0}_5^T & J_{5,7} \end{bmatrix} \begin{bmatrix} \dot{x}_t \\ \dot{y}_t \\ \dot{z}_t \\ \omega_{xt} \\ \omega_{zt} \\ \dot{q}_{t,7} \end{bmatrix} = \begin{bmatrix} J_{1,1} & & J_{1,6} & 0 \\ J_{2,1} & & J_{2,6} & 0 \\ J_{3,1} & \dots & J_{3,6} & 0 \\ J_{4,1} & & J_{4,6} & 0 \\ J_{6,1} & & J_{6,6} & 0 \\ -J_{5,1} & & -J_{5,6} & 1 \end{bmatrix} \begin{bmatrix} \dot{q}_{t,1} \\ \dot{q}_{t,2} \\ \dot{q}_{t,3} \\ \dot{q}_{t,4} \\ \dot{q}_{t,6} \\ \omega_{yt} \end{bmatrix} \tag{7b}$$

The following is the rearranged equation.

$$\begin{bmatrix} \dot{q}_{t,1} \\ \dot{q}_{t,2} \\ \dot{q}_{t,3} \\ \dot{q}_{t,4} \\ \dot{q}_{t,6} \\ \omega_{yt} \end{bmatrix} = \begin{bmatrix} J_{1,1} & & J_{1,6} & 0 \\ J_{2,1} & & J_{2,6} & 0 \\ J_{3,1} & \dots & J_{3,6} & 0 \\ J_{4,1} & & J_{4,6} & 0 \\ J_{6,1} & & J_{6,6} & 0 \\ -J_{5,1} & & -J_{5,6} & 1 \end{bmatrix}^{-1} \begin{bmatrix} & -J_{1,7} \\ & -J_{2,7} \\ \boldsymbol{I}_5 & -J_{3,7} \\ & -J_{4,7} \\ & -J_{6,7} \\ \boldsymbol{0}_5^T & J_{5,7} \end{bmatrix} \begin{bmatrix} \dot{x}_t \\ \dot{y}_t \\ \dot{z}_t \\ \omega_{xt} \\ \omega_{zt} \\ \dot{q}_{t,7} \end{bmatrix} \tag{7c}$$

Here, among the variables $\dot{x}_t, \dot{y}_t, \dot{z}_t, \omega_{xt}, \omega_{zt}, \dot{q}_{t,7}$, the term $\dot{z}_t$ can take an arbitrary value, while all other terms are set to zero. The desired joint angular velocity $\dot{\boldsymbol{q}}_t$ at the hit time is calculated as described above.

A first-order polynomial defines M2 trajectory to achieve a constant velocity towards the target as follows:

$$\boldsymbol{q}_d(t) = \boldsymbol{a}(t - T_b) + \boldsymbol{q}_{\text{ini}} \tag{8}$$
$$\dot{\boldsymbol{q}}_d(t) = \boldsymbol{a} \tag{9}$$

where $\boldsymbol{q}_d$ is the desired joint angle, $\boldsymbol{q}_{\text{ini}}$ is the initial joint angle, T_s is planned end time of M2.

The coefficients and initial joint angle $\boldsymbol{q}_{\text{ini}}$ are determined from the following constraint conditions:

$$\boldsymbol{q}_d(T_b) = \boldsymbol{q}_{\text{ini}} \tag{10}$$
$$\boldsymbol{q}_d(T_s) = \boldsymbol{q}_{\text{t}} \tag{11}$$

where T_s is the planned end time of M2. As a result, the coefficients are determined as follows:

$$\boldsymbol{a} = \dot{\boldsymbol{q}}_t \tag{12}$$
$$\boldsymbol{q}_{\text{ini}} = \boldsymbol{q}_t - \dot{\boldsymbol{q}}_t(T_s - T_b) \tag{13}$$

During this mode, the trajectory is tracked using a PD controller with an additional feedforward term to attenuate the reaction torque. The command torque $\boldsymbol{\tau}_m$ is;

$$\boldsymbol{\tau}_m = \boldsymbol{K}_p(\boldsymbol{q}_d - \boldsymbol{q}_s) + \boldsymbol{K}_d(\dot{\boldsymbol{q}}_d - \dot{\boldsymbol{q}}_s) + \boldsymbol{e}_7\alpha e^{-\gamma|t-(T_h - T_{h,\text{margin}})|} \tag{14}$$

where $\boldsymbol{q}_s$ is the measured joint angle and $\dot{\boldsymbol{q}}_s$ is the joint angular velocity; α is the peak value of the feedforward term; γ is the constant that adjusts the sharpness of the pulse; and $\boldsymbol{e}_7 = [0, 0, 0, 0, 0, 0, 1]^T$ is the basis vector that selects Joint 7. The parameter $T_{h,\text{margin}}$ is the time margin that determines how far in advance of the impact time T_h the peak of the feedforward term is applied. For example, if $T_{h,\text{margin}} = 2$ ms, the peak occurs 2 ms before impact.

C. Mode M1: Backswing Mode

To ensure a transition from the robot's initial posture $\boldsymbol{q}_{\text{ini}}$, M1 precedes M2. This mode uses a third-order polynomial to generate a preparatory motion over a duration T_b:

$$\boldsymbol{q}_d(t) = \boldsymbol{b}t^3 + \boldsymbol{c}t^2 + \boldsymbol{d}t + \boldsymbol{q}_{\text{ini}} \tag{15}$$
$$\dot{\boldsymbol{q}}_d(t) = 3\boldsymbol{b}t^2 + 2\boldsymbol{c}t + \boldsymbol{d}t \tag{16}$$

The coefficients are determined from the following boundary conditions, which define a motion that starts from rest at $\boldsymbol{q}_{\text{ini}}$, returns to $\boldsymbol{q}_{\text{ini}}$, and connects to M2's initial state:

$$\boldsymbol{q}_d(0) = \boldsymbol{q}_{\text{ini}} \tag{17}$$
$$\boldsymbol{q}_d(T_b) = \boldsymbol{q}_{\text{ini}} \tag{18}$$
$$\dot{\boldsymbol{q}}_d(0) = \boldsymbol{0} \tag{19}$$
$$\dot{\boldsymbol{q}}_d(T_b) = \boldsymbol{a} = \dot{\boldsymbol{q}}_t \tag{20}$$

As a result, the coefficients are determined as follows:

$$\boldsymbol{b} = \dot{\boldsymbol{q}}_t / T_b^2 \tag{21}$$
$$\boldsymbol{c} = -\dot{\boldsymbol{q}}_t / T_b \tag{22}$$
$$\boldsymbol{d} = \boldsymbol{0} \tag{23}$$

During this mode, the trajectory is tracked using a PD controller:

$$\boldsymbol{\tau}_m = \boldsymbol{K}_p(\boldsymbol{q}_d - \boldsymbol{q}_s) + \boldsymbol{K}_d(\dot{\boldsymbol{q}}_d - \dot{\boldsymbol{q}}_s) \tag{24}$$

D. Mode M3: Lift-up Mode

M3 is triggered when the measured torque at the 7th joint exceeds 0.1 Nm. In M3, the command torque is determined by the following equation:

$$\boldsymbol{\tau}_m = \boldsymbol{J}^T\boldsymbol{e}_z\beta e^{-\zeta(t-T_s)} + \frac{t - T_s}{T_l - T_s}(\boldsymbol{K}_p(\boldsymbol{q}_{\text{ini}} - \boldsymbol{q}_s) - \boldsymbol{K}_d\dot{\boldsymbol{q}}_s) \tag{25}$$

The first term, $\boldsymbol{J}^T\boldsymbol{e}_z\beta e^{-\zeta t}$, generates the initial lifting force. The Jacobian transpose, $\boldsymbol{J}^T$, converts task-space forces into

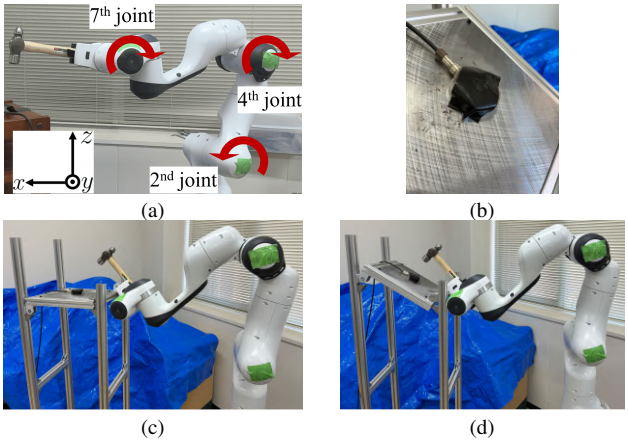

Fig. 4. Experimental Setup. (a) Franka Research 3. (b) Load-cell. (c) Environment of Ex. 1 and Ex. 2. (d) Environment of Ex. 3.

TABLE I
PD GAINS.

	$\boldsymbol{K}_p$	$\boldsymbol{K}_d$
Joint 1	1000 Nm/rad	50 Nm·s/rad
Joint 2	1000 Nm/rad	50 Nm·s/rad
Joint 3	1500 Nm/rad	50 Nm·s/rad
Joint 4	2500 Nm/rad	60 Nm·s/rad
Joint 5	750 Nm/rad	30 Nm·s/rad
Joint 6	700 Nm/rad	25 Nm·s/rad
Joint 7	600 Nm/rad	8 Nm·s/rad

TABLE II
THE PARAMETERS OF THE CONTROLLER.

	α [Nm]	β [Nm]	γ [1/s]	ζ[1/s]
Controller P1	10	60	420	100
Controller P2	10	30	420	100
Controller A	0	0	0	0
Controller B	0	60	0	100

joint torques. The basis vector $\boldsymbol{e}_z = [0,0,1,0,0,0]^T$ directs this force along the positive z-axis to lift the hammer. The peak value of the force is set by β, and it exponentially decays at a rate of ζ. This decay prevents a large, sustained command torque from destabilizing the robot's posture.

The second term is a PD controller, gradually ramped up by $(t-T_s)/(T_l-T_s)$, that guides the robot back to its initial posture $\boldsymbol{q}_{\text{ini}}$. T_l is the planned end time of M3.

IV. EXPERIMENTAL VALIDATION

A. Experiment Environment

Franka Research 3, a collaborative robot manufactured by Franka Robotics, was used for the experiments in this paper. Fig. 4 (a) shows the robot and some of its joints with their positive directions. The load cell used as the hammering target is shown in Fig. 4 (b), while the experimental setups for Experiment 1 and Experiment 2, and for Experiment 3 are shown in Fig. 4 (c) and (d), respectively. Franka Control Interface (FCI) provided by Franka Robotics was used to communicate between the robot and the PC, connecting the robot's controller to an external program and sending and receiving data every 1 ms.

The motion timeline was designed based on the planned end times for each mode: M1 ends at $T_b = 0.7$ s, M2 at $T_s = 0.85$ s, and M3 at $T_l = 1.15$ s. This plan incorporates an initial 0.2 s positioning phase, resulting in a duration for M1 of 0.5 s and a planned duration for M2 of 0.15 s. The planned time T_h of impact, which corresponds to the scheduled end of M2 ($T_h = 0.85$ s). However, the actual transition from M2 to M3 is triggered when the measured torque $\tau_{s,7}$ at the 7th joint exceeds 0.1 Nm. Consequently, the actual timing of this transition may differ from the plan. Table I summarizes the PD gains applied in Eqs. (14), (24), and (25), while Table II presents the corresponding parameters used in each experiment.

Controllers P1 and P2 include an additional feedforward term to the PD term during mode M2. In mode M3, a command torque is applied to lift up the hammer. With Controller A, the command torque in mode M2 is determined by the PD term, and it becomes zero in mode M3, meaning that the hammer is not lifted. With Controller B, the command torque in mode M2 is determined by the PD term, and in mode M3, a command torque is applied to lift up the hammer.

B. Experiment 1: After impact

Experiment 1 compares two cases: one in which the hammer was not lifted after impact and one in which it was. The objective is to verify if lifting the hammer can attenuate the torque on the joints while the force applied to the load cell remains approximately the same between the two cases. In both scenarios, the hammer strikes the load cell in the z-direction with a pre-impact velocity of -0.65 m/s. For this motion, the 2nd, 4th, and 7th joints were actuated, while the other joints were kept at their initial angles. Five trials were conducted for each of the two conditions.

The results of Experiment 1 are shown in Fig. 5. Fig. 5 (a) shows the measured and commanded torques for joints 2, 4, and 7 (from left to the right) for the case without lifting the hammer. Similarly, Fig. 5 (b) shows the torques for the case where the hammer was lifted. The measured torque is indicated by a solid line and the command torque by a dashed line. Fig. 5 (c) shows the force applied to the environment, as measured by a load cell.

These results confirm that lifting the hammer after a collision can effectively attenuate the reaction torques on the joints. Specifically, by comparing 5 (a) and 5 (b), one can see that the maximum measured torque at the fourth joint decreased from 12 Nm to 3 Nm, corresponding to an attenuation of approximately 75 %. One can also see that the maximum measured torque at the 7th joint decreased from 13 Nm to 11 Nm, which represents approximately a 15 % attenuation.

In spite of such reductions in the joint measured torques, the force applied to the environment remained nearly the same in both cases, as shown in Fig. 5 (c). This demonstrates that the proposed method can attenuate the forces

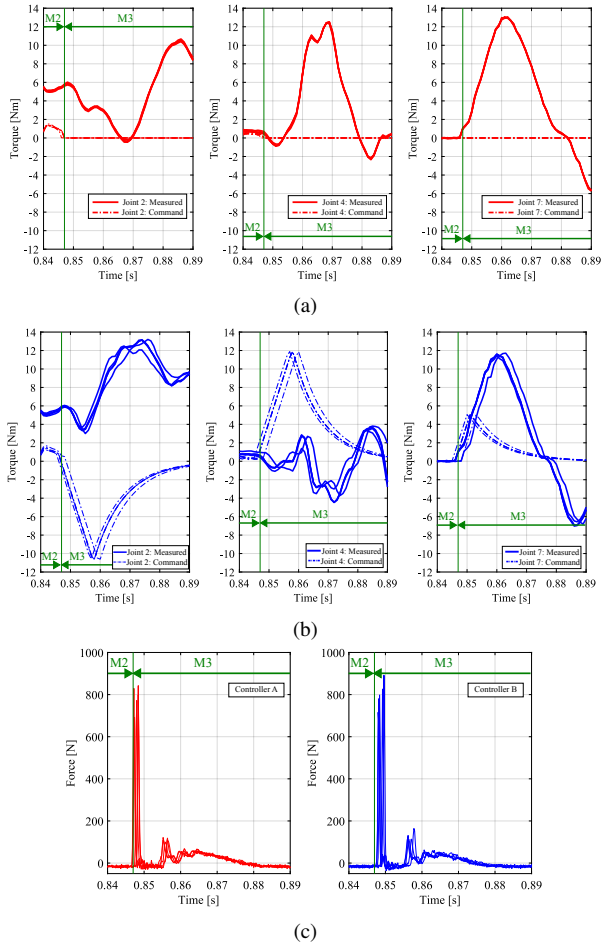

Fig. 5. Result of Experiment 1 (overlay of 5 trials). (a) Controller A. (b) Controller B. (c) Force applied to the load-cell (Comparison of Controller A and Controller B).

on the robot while maintaining the force delivered to the environment.

C. Experiment 2: Before impact

Experiment 2 compares two cases: one without a pre-collision feedforward torque and one with. The objective is to verify if applying this torque just before impact can attenuate the post-collision torque on the joints, while the force applied to the load cell remains approximately the same between the two cases. In both scenarios, the hammer strikes the load cell in the z-direction with a pre-collision velocity of -0.65 m/s. For this motion, the 2nd, 4th, and 7th joints were actuated, and the post-collision lift was enabled with its parameters set to $\beta = 60$ and $\zeta = 100$. Five trials were conducted for each condition.

The results of Experiment 2 are shown in Fig. 6. A comparison of the measured torques in Fig. 6 (a) and (b) shows that applying the pre-collision feedforward torque attenuates the maximum reaction torque on the 7th joint by approximately 25 %, specifically, reducing it from 12 Nm to 9 Nm. Moreover, the force applied to the environment remained nearly the same in both scenarios.

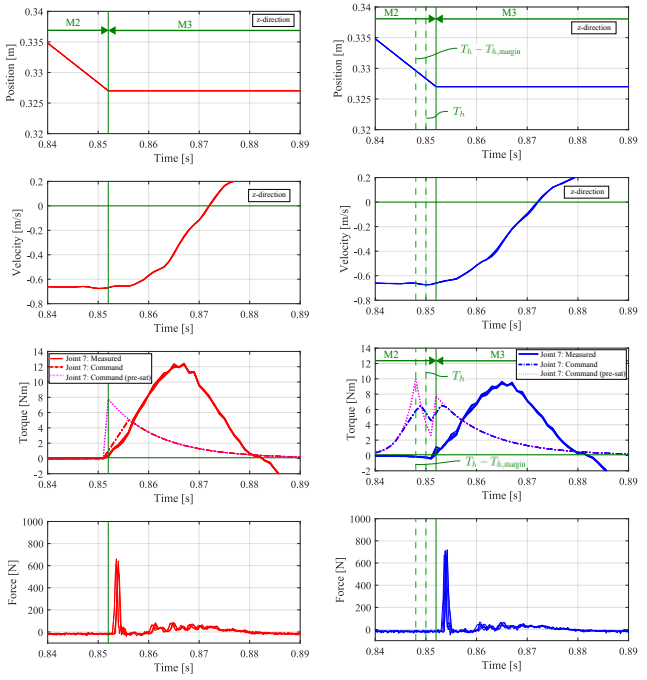

Fig. 6. Result of Experiment 2 (overlay of 5 trials). (a) Controller B. (b) Controller P1.

This outcome is explained by the central finding: A larger command torque input just before the hammer contacts the environment results in a smaller measured reaction torque after impact. This was achieved while the pre-collision hammer-tip velocity and the overall arm motion were kept consistent across two conditions, demonstrating that the method can attenuate the torque on the robot without compromising the hammering performance.

D. Experiment 3: Target on an angle

Experiment 3 investigates the method's performance on a non-horizontal target by placing the load cell on an inclined surface. The experiment again compares two cases: one without a pre-collision feedforward torque and one with. The objective is to verify that the method can still attenuate joint torques while maintaining a consistent impact force, even when the target surface is not level. For both cases, the hammer strikes the load cell in the z-direction with a pre-collision velocity of -0.65 m/s, the 2nd, 4th, and 7th joints were actuated. Five trials were condsucted for each condition.

The results of Experiment 3 are shown in Fig. 7. A comparison of the measured torques in Fig. 7 (a) and (b) shows that applying the pre-collision feedforward torque attenuates the maximum reaction torque on the 7th joint by approximately 33 %, specifically, from 9 Nm to 6 Nm. Moreover, the force applied to the environment remained nearly the same in both scenarios.

This outcome is that the method can also attenuate the reaction torque when the load cell is placed on an inclined surface.

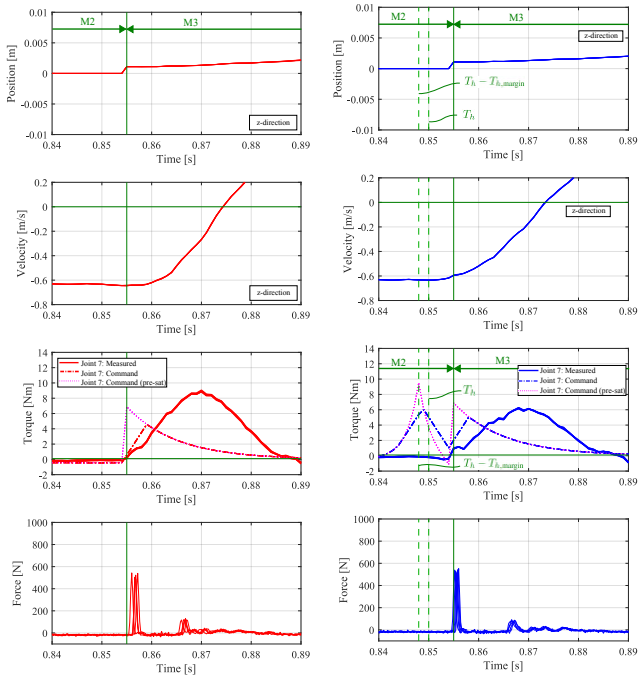

(a) (b)

Fig. 7. Result of Experiment 3 (overlay of 5 trials). (a) Controller B. (b) Controller P2.

V. Conclusion

This paper has proposed a control method for robotic hammering designed to attenuate the trade-off between delivering a large impact to the environment and suppressing the reaction torques on the robot's joints. The method is based on a trajectory generation scheme that plans the motion by calculating backward in time from a desired state at impact. This trajectory is combined with a feedforward torque pulse applied just before contact to attenuate reaction torques.

The proposed strategies were validated through experiments, which demonstrated a reduction in joint torques. The post-impact lift-up strategy first attenuated reaction torques by approximately 75 % at the 4th joint and 15 % at the 7th joint. The addition of the pre-impact feedforward strategy then provided a further 25 % reduction at the 7th joint. Importantly, the force delivered to the environment remained consistent across all tested scenarios. These findings indicate that the proposed method can enhance the safety and durability of robots performing tasks involving impacts.

Further development toward practical application should focus on applying the method to a wider range of tasks and implementing adaptive algorithms for the feed-forward controller to handle environments with varying stiffness.

References

[1] N. Dehio, Y. Wang, and A. Kheddar, "Dual-arm box grabbing with impact-aware MPC utilizing soft deformable end-effector pads," IEEE Robotics and Automation Letters, vol. 7, no. 2, pp. 5647-5654, 2022.

[2] Y. Wang, N. Dehio, and A. Kheddar, "Predicting impact-induced joint velocity jumps on kinematic-controlled manipulator," IEEE Robotics and Automation Letters, vol. 7,no. 3, pp. 6226–6233, 2022.

[3] J. van Steen, G. van den Brandt, N. van de Wouw, J. Kober, and A. Saccon, "Quadratic programming-based reference spreading control for dual-arm robotic manipulation with planned simultaneous impacts," IEEE Transactions on Robotics, vol. 40, pp. 3341–3355, 2024.

[4] K. Li, X. Xiong, A. Wang, Y. Qu, and Y. Lou, "Implicit Euler Discrete-Time Set-Valued Admittance Control for Impact–Contact Force Control," IEEE/ASME Transactions on Mechatronics, pp. 1–12, 2024.

[5] R. Kikuuwe, "Dynamics modeling of gear transmissions with asymmetric load-dependent friction," Mechanism and Machine Theory, vol. 179, no. 3, pp. 105–116, Jul. 2023.